ELSEVIER

Journal of Environmental Management 85 (2007) 638–648

Journal of Environmental Management

www.elsevier.com/locate/jenvman

LAI inversion algorithm based on directional reflectance kernels

S. Tang[a,b,*], J.M. Chen[c], Q. Zhu[b], X. Li[b], M. Chen[c], R. Sun[b], Y. Zhou[b], F. Deng[c], D. Xie[b]

[a]*Key Laboratory of Radiometric Calibration and Validation for Environmental Satellites National Satellite Meteorological Center, China Meteorological Administration, Beijing 100081, China*

[b]*Remote Sensing and GIS Research Center, Department of Geography, Beijing Normal University, Beijing 100875, China*

[c]*Department of Geography and Program in Planning, University of Toronto, 100 St. George St., Room 5047,Toronto, ON, Canada M5S 3G3*

Received 15 April 2004; received in revised form 6 December 2005; accepted 23 August 2006
Available online 28 November 2006

Abstract

Leaf area index (LAI) is an important ecological and environmental parameter. A new LAI algorithm is developed using the principles of ground LAI measurements based on canopy gap fraction. First, the relationship between LAI and gap fraction at various zenith angles is derived from the definition of LAI. Then, the directional gap fraction is acquired from a remote sensing bidirectional reflectance distribution function (BRDF) product. This acquisition is obtained by using a kernel driven model and a large-scale directional gap fraction algorithm. The algorithm has been applied to estimate a LAI distribution in China in mid-July 2002. The ground data acquired from two field experiments in Changbai Mountain and Qilian Mountain were used to validate the algorithm. To resolve the scale discrepancy between high resolution ground observations and low resolution remote sensing data, two TM images with a resolution approaching the size of ground plots were used to relate the coarse resolution LAI map to ground measurements. First, an empirical relationship between the measured LAI and a vegetation index was established. Next, a high resolution LAI map was generated using the relationship. The LAI value of a low resolution pixel was calculated from the area-weighted sum of high resolution LAIs composing the low resolution pixel. The results of this comparison showed that the inversion algorithm has an accuracy of 82%. Factors that may influence the accuracy are also discussed in this paper.

Keywords: LAI; MODIS; BRDF; Albedo; Gap fraction

1. Introduction

Leaf area index (LAI) is defined as one half the total green leaf area (all sided) per unit ground surface area (Chen and Black, 1992). It is an important parameter of terrestrial ecosystems, and represents the amount of the surface area at the interface between plant canopy and the atmosphere for the fluxes of energy, mass (e.g., water and CO_2), and momentum. Estimating LAI is therefore important for estimating evapotranspiration, net primary productivity, and crop yields, and is also useful for studies of regional and global changes.

Several methods have been developed to estimate LAI from remote sensing data (Weiss and Baret, 1999), which can be grouped into two main classes:

(1) *Empirical relationships based on vegetation indices*. This method correlates LAI with a vegetation index, typically a combination of reflectances observed in different spectral bands under one viewing direction. The most commonly used vegetation indices at the present are the normalized difference vegetation index (NDVI) and simple ratio (SR) index. However, the abilities of NDVI and SR in retrieving LAI are affected by the background of the vegetation. In addition, since most indices often become saturated at high LAI values, the LAI retrieval loses accuracy for dense canopies. The empirical relations between LAI and NDVI or SR are generally non-linear and vary with location, time, as well as vegetation type. Since it is

*Corresponding author. National Satellite Meteorological Center, China Meteorological Administration, Beijing 100081, China.
Tel.: +86 10 68407250; fax: +86 10 68407250.
E-mail addresses: tshyjf@yahoo.com.cn, tangshh@nsmc.cma.gov.cn (S. Tang).

0301-4797/$ - see front matter © 2006 Elsevier Ltd. All rights reserved.
doi:10.1016/j.jenvman.2006.08.018

impossible to directly measure LAI over large areas on the ground, large errors are introduced if such empirical relations are derived from high resolution images and then applied to coarse resolution images (Chen, 1999). In addition, compared with other approaches, vegetation index-based methods can only use part of the information obtainable from remote sensing.

(2) *Model based on inversions*. Remote sensing model inversions consist of determining a set of canopy biophysical variables that minimizes the difference between simulated and observed reflectances at various spectral bands. These inversion model parameters have definite physical meaning, so this method is increasingly used in current studies. The precision of a model-based inversion depends on the modeling methodology. Four classes of models may be distinguished according to their theoretical basis: turbid medium, geometric optical, hybrid, and stochastic simulation models (Goel, 1988). Model inversions can be achieved using various methods including the traditional iteration methods, lookup tables, and hybrid methods (e.g., neural network method). Traditional iteration methods are time-consuming, and therefore not suitable for pixel-by-pixel inversions. For processing large data sets, simplification of models or algorithms is necessary, but this inevitably decreases the inversion accuracy.

Lookup table methods can partly overcome the drawbacks of iteration methods. A lookup table is built in advance through forward calculations to connect parameters to be inverted to reflectances. During an inversion, only search and interpolation operations are needed within a pre-established table. However, to reach high accuracy, the dimension of the table must be large enough, which will decrease the on-line searching speed. Moreover, some parameters, such as soil reflectance, leaf reflectance, etc., need to be specified in advance. These parameters are replaced by their representative values, whereas they sometimes may not only be highly variable but also have great influence on reflectance.

Hybrid methods are the combination of remote sensing models and non-parametric statistical inversion methods. Simulation data produced from remote sensing forward models and non-parametric statistical methods (e.g. neural networks, local regression) are used to build the connection between directional reflectances and the parameters to be inverted. Compared with lookup table methods, the main advantage of hybrid methods is the ability to explain the fluctuations of key parameters. Although many variables are needed to produce simulation data, hybrid methods can connect model outputs with several key input parameters. This is because non-parametric statistical methods have the ability to transform data through a non-linear projection, and to enhance some factors while compressing others.

Although reflectance models are generally mathematically invertible, they do not provide a complete description of the actual radiative transfer and canopy structure. Further, a measured reflectance value often has a large confidence interval. Therefore, the inverse solution is not always unique, as a different set of physical variables may yield very similar directional or spectral signature (Weiss and Baret, 1999).

Given the importance of LAI and the limitations to its retrieval from one-directional measurements, it is important to evaluate the added contribution of directional remote sensing for LAI retrieval. The objective of this paper is to develop a simple method that applies directional information to retrieving LAI.

2. Algorithm description

2.1. Calculation principles for LAI

LAI can be expressed as the product$\mathrm{LAI} = \mu * z$. of leaf area density (μ, in $\mathrm{m^2\,m^{-3}}$) and canopy height (z, in m):

$$\mathrm{LAI} = \mu * z. \tag{1}$$

In a horizontally homogeneous canopy with randomly distributed, infinitely thin, planar leaves, the mean gap probability in direction θ_v can be expressed as an exponential function of the optical path length $S(\theta_v)$, the leaf area density μ, and the fraction of foliage projected towards the direction θ_v, $G(\theta_v)$ (Broadhead et al., 2003):

$$T(\theta_v) = \exp(-G(\theta_v)\mu S(\theta_v)), \tag{2}$$

where $T(\theta_v)$ is the mean gap probability. Eq. (2) can be rewritten as

$$G(\theta_v)\mu = -\frac{\ln T(\theta_v)}{S(\theta_v)} = K(\theta_v), \tag{3}$$

where $K(\theta_v)$ is the average number of contacts per unit length of travel that a probe would make passing through the canopy at zenith angle θ_v (Welles and Norman, 1991).

The analytical solution for foliage density is given by Miller (1967) as

$$\mu = 2\int_0^{\pi/2} K(\theta_v)\sin\theta_v\,\mathrm{d}\theta_v. \tag{4}$$

The optical path length is related to the zenith angle by

$$S(\theta_v) = z/\cos(\theta_v). \tag{5}$$

The expression of LAI can be derived from μ and z:

$$\mathrm{LAI} = -2\int_0^{\pi/2} \ln(T(\theta_v))\cos\theta_v\,\sin\theta_v\,\mathrm{d}\theta_v. \tag{6}$$

In general, measurements are made at multiple angles (θ_{vi}, $i = 1, \ldots, m$, where m is the number of zenith angles used during the measurement). Therefore, the LAI can be computed using the discrete approximation as

follows:

$$\mathrm{LAI} = -2\sum_{i=1}^{m}\ln(T(\theta_{vi}))\sin\theta_{vi}\cos\theta_{vi}\Delta\theta_{vi} = -2\sum_{i=1}^{m}\left(\frac{1}{n}\sum_{j=1}^{n}\ln\big(T(\theta_{vij})\big)\right)\cos\theta_{vi}\sin\theta_{vi}\Delta\theta_{vi}, \quad (7)$$

where n is the number of azimuth angles. The gap probabilities in Eq. (7), averaged over the azimuth, represent mean values for the area seen by each detector. Lang and Xiang (1986) showed that if the canopy consists of homogeneous regions with different leaf area densities, averaging the transmittance over these regions would underestimate the LAI. Hence the average of logarithmic transmittances is used to substitute the logarithm of average transmittance in Eq. (7).

The LAI calculated from Eq. (7) should be an effective LAI, i.e., the part which directly contributes to the canopy interception of incident radiation (Chen and Black, 1991).To acquire actual LAI, the spatial clumping of leaf elements such as leaf or shoot, shoud be considered. The relationship between the effective LAI (L_e) and the total LAI L_t is given by (Chen and Cihlar, 1995a, b):

$$L_e = L_t \times \Omega, \quad (8)$$

where Ω is the clumping index determined by the spatial distribution pattern of the foliage elements. When the foliage spatial distribution is random, Ω is unity. If leaves are regularly distributed (extreme case: leaves are all laid side by side), Ω is larger than unity. When leaves are clumped (extreme case: leaves are stacked on top of each other), Ω is less than unity. The typical clumping index values for different land cover types are determined according to the suggested values of Myneni (adopted in his DISORD program) and Chen (adopted in his LAI algorithm which is developed for the VEGETATION sensor, Table 1).

The above derivation implies that LAI can be estimated from the distribution of gap probability over the upper hemisphere. In ground observations, the gap probability can be treated as the ratio between the corresponding below- and above-canopy radiation using upward facing sensors. The gap probability information can also be obtained from remote sensing above the canopy, using another approach.

Studies show that there is a good positive correlation between NDVI and crown cover fraction. However, after the crown cover fraction reaches a certain value, NDVI varies slowly. Multiangular remote sensing provides NDVI values at various angles, therefore it can be used to derive the canopy gap fraction at various angles. The directional gap fractions (i.e., at various satellite view angles) can be related to directional NDVIs according to the following equation (Baret et al., 1995; Gutman and Ignatov, 1998; Zeng et al., 2000):

$$T(\theta,\vartheta,\phi) = 1 - \frac{\mathrm{NDVI}(\theta,\vartheta,\phi) - \mathrm{NDVI}_{back}(\theta,\vartheta,\phi)}{\mathrm{NDVI}_{sat}(\theta,\vartheta,\phi) - \mathrm{NDVI}_{back}(\theta,\vartheta,\phi)}, \quad (9)$$

where NDVI_{sat} is the saturated NDVI, defined as the NDVI for vegetation fully occupying the field of view; NDVI_{back} is the NDVI of background under vegetation cover; θ is the solar zenith angle; ϑ is the view zenith angle, and ϕ is the relative azimuth angle between the sun and the satellite sensor. Global vegetation products from the Moderate Resolution Imaging Spectroradiometer (MODIS) provide the anisotropic reflectance information of surfaces, which consequently makes it possible to obtain the directional gap fraction for each pixel.

Table 1
Clumping Index for different IGBP land cover types

IGBP Class	Class name	Clumping index (Chen)	Class (Myneni)	Clumping index (Myneni)	Clumping index (this paper)
1	Evergreen needleleaf forest	0.6	Needle forest	0.6	0.6
2	Evergreen broadleaf forest	0.8	Leaf forest	0.8	0.8
3	Deciduous needleleaf forest	0.6	Needle forest	0.6	0.6
4	Deciduous broadleaf forest	0.8	Leaf forest	0.8	0.8
5	Mixed forest	0.7			0.7
6	Closed shrublands	0.5	Shrublands	1.0	0.8
7	Open shrublands	0.5	Shrublands	1.0	0.8
8	Woody savannas	0.5	Savanna	0.8	0.8
9	Savannas	0.5	Savanna	0.8	0.8
10	Grasslands	0.9	Grasses/cereal crop	1.0	0.9
11	Permanent wetlands	0.9			0.9
12	Croplands	0.9	Broadleaf crops	1.2	0.9
13	Urban and built-up	0.9			0.9
14	Cropland mosaics	0.9			0.9

2.2. Reconstruction of bidirectional reflectance from MODIS BRDF parameters

A global set of parameters describing the bidirectional reflectance distribution function (BRDF) of the land surface is available in the MODIS BRDF/ALBEDO Products (MOD43B1). These products are derived from multidate, atmospherically corrected, and cloud-cleared data over 16-day periods with a semi-empirical kernel-driven bidirectional reflectance model.

The semi-empirical kernel-driven bidirectional reflectance model adopted in the MODIS product is also known as a parameterization model. The theoretical basis of the semi-empirical models is that the surface reflectance can be modeled as a sum of three kernels representing three basic scattering types (Roujean et al., 1992; Lucht et al., 2000):

$$R(\theta,\vartheta,\phi,\Lambda) = f_{\mathrm{iso}}(\Lambda)K_{\mathrm{iso}} + f_{\mathrm{vol}}(\Lambda)K_{\mathrm{vol}}(\theta,\vartheta,\phi) + f_{\mathrm{geo}}(\Lambda)K_{\mathrm{geo}}(\theta,\vartheta,\phi), \quad (10)$$

where K_{iso} stands for the isotropic kernel and is a constant of unity; $K_{\mathrm{vol}}(\theta,\vartheta,\phi)$ is the volumetric scattering kernel, which describes the contribution of horizontally homogeneous leaf canopies; and $K_{\mathrm{geo}}(\theta,\vartheta,\phi)$ is the geometric-optical surface scattering kernel, which describes the contribution of 3-D objects that cast individual and mutual shadows at off-nadir view angles; f_{iso}, f_{vol}, and f_{geo} are the weights given to the corresponding kernels, respectively. The volume-scattering term can be considered as the effects caused by the small (interleaf) gaps in a canopy, whereas the geometric-optical term is caused by the larger (inter-crown) gaps.

There are many expressions and combinations for the geometric-optical kernel and the volumetric scattering kernel (Walthall et al., 1985; Roujean et al., 1992; Li and Strahler, 1992; Gao et al., 2001). Studies show that the combination of Ross-Thick and Li-SparseR kernels works well with the observed data (Lucht et al., 2000), and the model parameters of this combination are provided in the MODIS BRDF/albedo product.

The Ross-Thick kernel is a single-scattering approximation of the radiative transfer theory proposed by Ross (1981) consisting of a layer of small scatterers with a random leaf angle distribution, a Lambertian background, and equal leaf transmittance and reflectance. The form of Ross-Thick kernel is (Roujean et al., 1992):

$$K_{\mathrm{vol}} = K_{\mathrm{RT}} = \frac{(\pi/2-\xi)\cos\xi + \sin\xi}{\cos\theta + \cos\vartheta} - \frac{\pi}{4}, \quad (11)$$

where ξ is the phase angle defined as

$$\xi = \arccos(\cos\theta\cos\vartheta + \sin\theta\sin\vartheta\cos\phi). \quad (12)$$

The Li-SparseR kernel was derived from the geometric optical mutual shadowing BRDF model by Li and Strahler (Li and Strahler, 1992; Wanner et al., 1995):

$$K_{\mathrm{geo}} = k_{\mathrm{LSR}} = O(\theta,\vartheta,\phi) - \sec\theta' - \sec\vartheta' + \frac{1}{2}(1+\cos\xi')\sec\theta'\sec\vartheta', \quad (13)$$

where O is the overlap area between the view and solar shadows, which is computed from

$$O = \frac{1}{\pi}(t - \sin t\cos t)(\sec\theta' + \sec\vartheta'), \quad (14)$$

where

$$\cos t = \frac{h}{b}\frac{\sqrt{D^2 + (\tan\theta'\tan\vartheta'\sin\phi)^2}}{c'\theta + \sec\vartheta'}, \quad (15)$$

$$D = \sqrt{\tan^2\theta' + \tan^2\vartheta' - 2\tan\theta\tan\vartheta'\cos\phi}, \quad (16)$$

and $\cos\xi'$, θ', and ϑ' can be calculated as

$$\cos\xi' = \cos\theta'\cos\vartheta' + \sin\theta'\sin\vartheta'\cos\phi'), \quad (17)$$

$$\theta' = \tan^{-1}\left(\frac{b}{r}\tan\theta\right), \quad (18)$$

$$\vartheta' = \tan^{-1}\left(\frac{b}{r}\tan\vartheta\right), \quad (19)$$

where h/b and b/r are dimensionless parameters, which describe the crown relative height and shape factors. They are often given the values of 2 and 1, respectively, which means that spherical crowns are separated from the ground by half their diameter. Using the parameters provided in the MODIS land product (MOD43B1) and the above model, we can reconstruct the anisotropic effect of a surface.

2.3. LAI inversion procedure based on MODIS BRDF/ALBEDO product

Fig. 1 shows a schematic diagram of our LAI inversion procedure based on the MODIS BRDF/ALBEDO product. The module for determining saturated and background NDVI values, marked with the dashed line in Fig. 1, needs to be run only once. The BRDF model parameters are obtained from MOD43B1, and then BRDF is calculated according to the Ross-Thick and Li-SparseR kernel model (Eqs. (10)–(19)). The directional NDVI is calculated according to Eq. (20):

$$\mathrm{NDVI}(\theta,\vartheta,\phi) = \frac{(\mathrm{BRDF}_{\mathrm{ir}}(\theta,\vartheta,\phi) - \mathrm{BRDF}_{\mathrm{r}}(\theta,\vartheta,\phi))}{(\mathrm{BRDF}_{\mathrm{ir}}(\theta,\vartheta,\phi) + \mathrm{BRDF}_{\mathrm{r}}(\theta,\vartheta,\phi))}, \quad (20)$$

where $\mathrm{BRDF}_{\mathrm{ir}}$ and $\mathrm{BRDF}_{\mathrm{r}}$ are BRDF values in the red and near infrared bands, respectively. The canopy NDVI should be between $\mathrm{NDVI}_{\mathrm{back}}$ and 1. Because of the influence of the background or data errors, NDVI may be less than $\mathrm{NDVI}_{\mathrm{back}}$ or greater than 1. When $\mathrm{NDVI} < \mathrm{NDVI}_{\mathrm{back}}$, we set $\mathrm{NDVI} = \mathrm{NDVI}_{\mathrm{back}}$, which

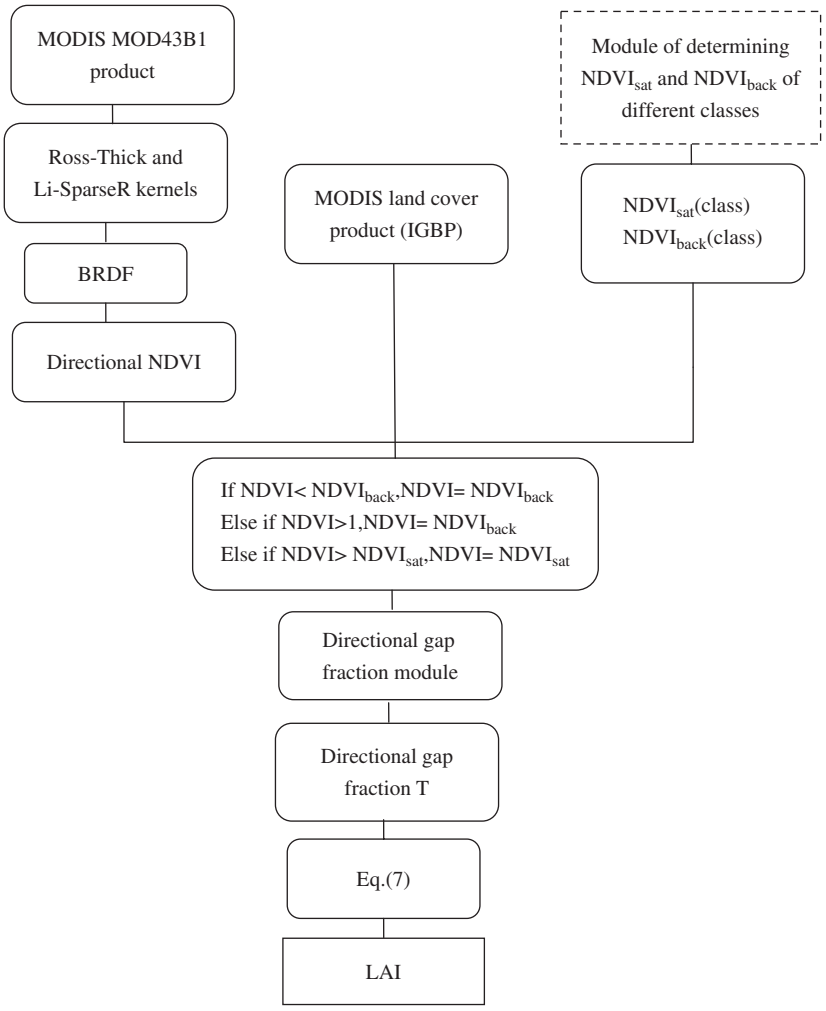

Fig. 1. Flow diagram of the inversion procedure.

means that NDVI in this case is determined mainly by the background, and the gap fraction is 1. When NDVI > $NDVI_{sat}$, the sensor field of view is fully covered by the canopy, and we set NDVI = $NDVI_{sat}$.

Gap fraction is calculated using Eq. (9), and LAI is inverted according to Eq. (7). Similar to the ground measurements using LAI-2000, the MODIS BRDF products are unreliable at high zenith angles. Results from any simple BRDF model should generally be treated with caution for zenith angles larger than 80° or so (Strahler et al., 1999). In Eq. (7), $\sum_{i=1}^{m} \sin\theta_{vi}\Delta\theta_{vi} = 1$ i.e. $\int_0^{\pi/2} \sin\theta_{vi}\,d\theta_{vi} = 1$, signifying a weighting operation for measurements at various zenith angles. The θ_v and $\Delta\theta_{vi}\sin\theta_{vi}$ values used in LAI-2000 are listed in Table 2 (Li-Cor, 1992).

Table 2 shows that the average angular integration step used in LAI-2000 is 15°, and the largest zenith angle range is 60–74°. The same integration steps and angle configuration can be used in our algorithm to improve calculation speed. We use the view zenith angle range from 0° to 75° with a 15° integration step; this scheme is similar to that of LAI-2000 (see Table 2).

Table 2
Parameters value for the LAI2000 LAI computation

θ_{v_i} (deg.)	$\Delta\theta_{vi}\sin\theta_{v_i}$
7	0.034
23	0.104
38	0.160
53	0.218
68	0.494

2.4. Determination of the saturated and background NDVI

Theoretically, for each canopy type and each solar and view angle configuration, there should be one pair of saturated and background NDVI values. For the same canopy type, since the saturation and background NDVI values vary less than 20% with view and illumination angles except for a small angular range near the hotspot (Leblanc et al., 1997), we only determine one land-cover dependent pair of saturation and background NDVI

values. It should also be pointed out that the saturation NDVI mentioned here refers to the NDVI value when the field of view is completely covered by the canopy, which is equivalent to the saturation point of NDVI. Even when the field of view is fully occupied by vegetation, NDVI may still increase slowly with view zenith angle due to the effects of multiple scattering.

As discussed later, the background NDVI has little influence on the accuracy of LAI inversion. Studies show that the range of background NDVI is generally between 0.02 and 0.05 (Baret et al., 1995; Gutman and Ignatov, 1998; Zeng et al., 2000). Based on our measurements, we found that background NDVI set to 0.02 would be suitable for our study in most cases.

The saturation NDVI can be acquired from experiment or model simulations, or from statistics of actual directional NDVI values. A model can first simulate the LAI–NDVI relation curves for different land covers and then determine the saturation NDVI according the curve shape; this method is simple and quick. The statistical method calculates maximal directional NDVI histogram of the same land cover, then takes 90% of the maximal NDVI as the saturation NDVI; theoretically, this method is more reliable, but it needs enough samples and is computationally intensive.

To determine the saturation NDVI for each IGBP land cover, the following method was used: directional NDVI values of each pixel are calculated from BRDF products, and then the maximal NDVI value of each pixel is found. The frequency of maximal NDVI values of each IGBP land cover is calculated, and the histogram is drawn. The NDVI value of the intersection point of the histogram and x-axis is taken as maximal NDVI of that land cover. Saturation NDVIs are assumed to be 90% of the maximal NDVIs.

The 5-Scale model (Chen and Leblanc, 1997; Leblanc et al., 1999; Leblanc and Chen, 2000) was used to test the saturation NDVI acquired from the above method. 5-Scale is a combination of 4-Scale model (Chen and Leblanc, 1997) and LIBERTY (Dawson et al., 1998). Its main goal is to compute the reflectance of a vegetated surface from the remote sensing. 5-Scale is a geometric-optical radiative-transfer model with emphasis on the structural composition of forest canopies at different scales. A multiple scattering scheme, which is capable of including the effect of canopy architecture on multiple orders of scattering, was incorporated into the model (Chen and Leblanc, 2001). Although developed for boreal forest (Leblanc et al., 1999), 5-Scale can also be applied to other types of vegetation. The directional reflectances of 15 IGBP land covers were simulated with their representative structural and spectral values using 5-Scale. By adjusting the reflectance of foliage and background, increasing 25% and decreasing 25% on the basis of average values respectively, we obtained the range of saturation NDVI. Fig. 2 illustrates the saturation NDVI determined from histogram and its range determined through 5-Scale simulations. It can readily be seen that all saturation NDVIs determined from the histogram method fall within the ranges determined by the 5-Scale model.

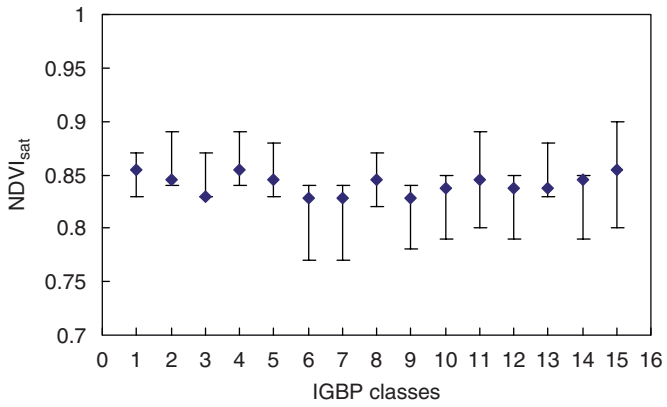

Fig. 2. Saturation NDVI of each IGBP land cover and its range.

3. Validation

3.1. LAI distribution map of China

The above algorithm was used to retrieve a LAI map of China in mid-July 2002. Fig. 3 is a false color composite image of that region, and its corresponding LAI map is illustrated in Fig. 4.

3.2. Study area

Field LAI measurements were made in two study areas: the Changbaishan Nature Reserve, in northeast China, and the Qilian Mountain in the upper reach of Heihe River, in northwest China.

The Changbaishan Nature Reserve was the main study area, located in the southeast of Jilin province, China

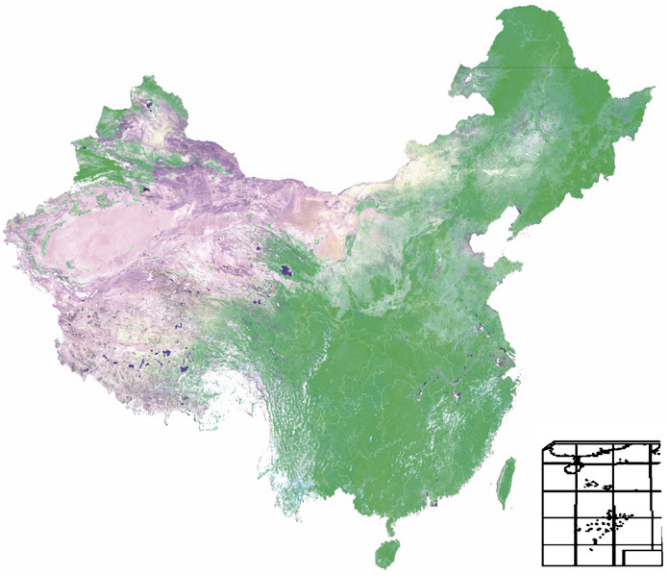

Fig. 3. Original false color composite image of China.

(41°42′N–42°10′N, 127°38′E–128°10′E) (Fig. 5). Its elevation ranges from 720 to 2691 m above sea level. The climate is temperate continental mountainous type. The annual rainfall is about 700 mm at lower levels and increases to about 1400 mm at Tianchi Lake, near the top of the Changbai Mountain. The mean annual air temperature varies from 4.9 °C at the foot of the mountain to −7.3 °C at its top.

Influenced by climate, the vegetation distribution varies with altitude in the region. Four landscape zones can be distinguished from 720 to 2600 m: Korean pine and broadleaf mixed forest zone (720–1100 m); dark coniferous forest zone (1100–1700 m), which dominated by conifers such as Korean pine, spruce, fir, and larch; subalpine *Betula ermanii* forest zone (1700–2000 m), representing a transition from dark coniferous forest to alpine tundra zone with birch as dominant but spruce, fir, larch, *Alnus maritime*, etc. also present; and alpine tundra zone (above 2000 m, no forest in this zone). The Korean pine and broadleaf mixed forest is the dominant vegetation type in this area. Its vegetation density varies with elevation, which provides a large natural range for developing remote sensing algorithms of biophysical parameters.

The Qilian Mountain study area lies in the Yugu nationality autonomous county, Gansu province, China, in the upper reach of Heihe River. The climate is semiarid with mean annual air temperature 0.5 °C, the annual rainfall of 440 mm, and the frost-free period 90–120 days long. Vegetation varies with climate and terrain, and can be divided into three zones: mountainous prairie-timber zone, subalpine brush and partum zone, and subalpine nival sparse vegetation zone. Mountainous prairie-timber zone is the main cover type, with *Picea crassifolia* as the dominant tree species.

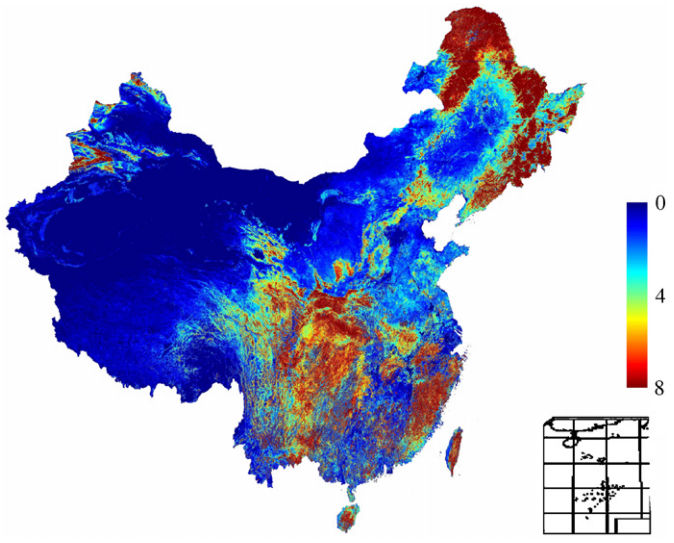

Fig. 4. LAI map in China in the middle of July 2002.

3.3. Site description and distribution

With few exceptions, the Changbai Mountain sampling sites were located within the Nature Reserve. The sites were distributed along an altitudinal gradient and included the main forest types. For each forest type, 3–5 sites with different stand densities were selected, guided by a satelllite image (Fig. 6). Table 3 shows the dominant forest type at each site.

There are 12 sampling sites at Qilian Mountain study area. They are distributed along Heihe River, and contain Qinghai spruce (*Picea crassifolia*) as the dominant tree species.

3.4. Experimental methods

The optical instrument named Tracing Radiation and Architecture of Canopies (TRAC) was used for measuring

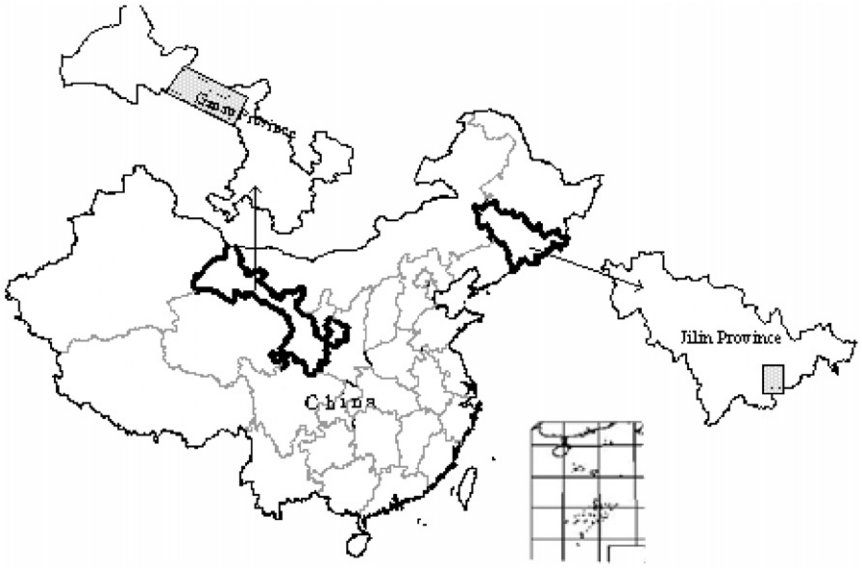

Fig. 5. Study areas.

LAI and the clumping index. The principles of TRAC and its use can be found in Chen and Cihlar (1995a, b) and Leblanc et al. (2002).

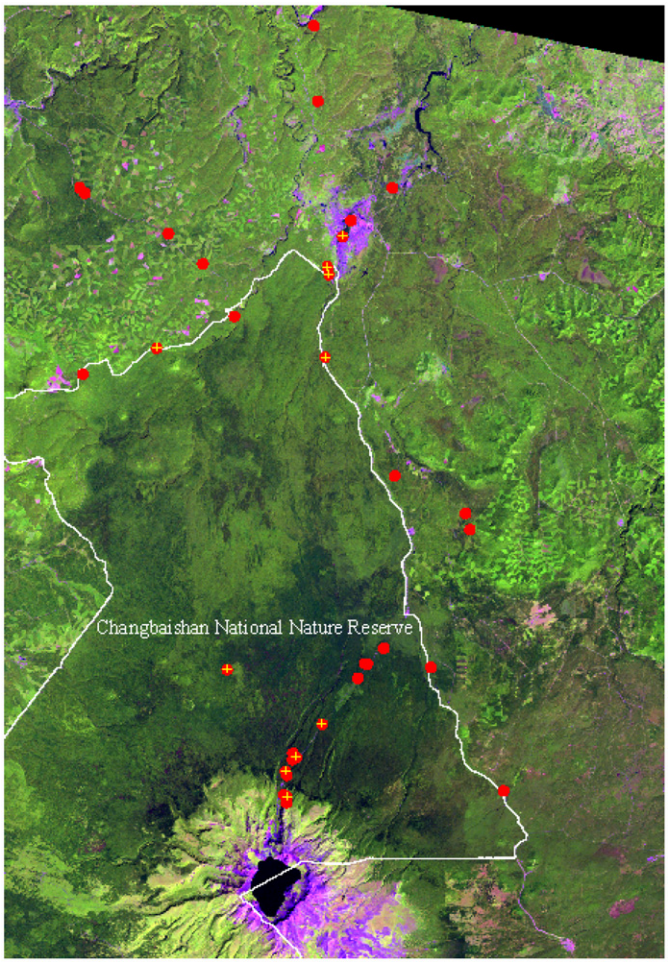

Fig. 6. Distribution of test sites in Changbai Mountain study area.

At each site, a 30 m × 30 m quadrant was selected. Three transects perpendicular to the sun's azimuth angle were set up in the quadrant. A forestry flag was inserted into the ground every 10 m along the transects to serve as a distance marker. Basic information on the test site was recorded including stand ID, position, slope and aspect, elevation, tree number, tree ring count, etc. The within-shoot clumping factor, required for TRAC measurements for conifer stands was taken from Chen et al. (1997) for similar species.

3.5. Validation methods

Because the resolution of a MODIS pixel is 1 km, it is impossible to directly relate a MODIS product to the ground measurements. In this paper, the high-resolution images whose pixel size is approximately equal to the ground plot size were used to scale up from ground sites to MODIS pixels. Two TM images acquired near the ground measurements period were chosen for this purpose, and treated as illustrated in Fig. 7. Scaling between small-plot ground measurements and low-resolution remote sensing data was achieved through the following steps:

(1) Empirical relationships were developed between vegetation indices and LAI measured on the ground, after the images were geometrically and radiometrically corrected and the digital numbers were converted to reflectance.
(2) High resolution LAI distributions were calculated using the above empirical relationships.
(3) The high resolution LAI images were co- registered with MODIS images.
(4) The mean LAI value for each MODIS pixel was calculated through arithmetic averaging of the high-resolution LAI values for all pixels that fall within each MODIS pixel.

Table 3
Site description

Stand ID	Forest type	Stand ID	Forest type
1	Broadleaf mixed forest	18	Korea pine and broadleaf forest
2	Broadleaf mixed forest	19	Larch forest
3	Larch forest	20	Cloudy fir forest
4	Bueaty pine forest	21	Korea pine and Cloudy fir forest
5	Bueaty pine forest	22	Poplar birch forest
6	Korea pine and broadleaf forest	23	Cloudy fir forest
7	Poplar birch forest	24	Needle and broadleaf mixed forest
8	Korea pine and broadleaf forest	25	Larch forest
9	Poplar birch forest	26	Larch and fir forest
10	Korea pine and broadleaf mixed forest	27	Cloudy fir forest
11	Korea pine forest	28	Cloudy fir forest
12	Broadleaf culled forest	29	Fir and Ermans Birch mixed forest
13	Korea pine forest	30	Cloudy fir forest
14	Korea pine and broadleaf forest	31	Fir and Ermans Birch mixed forest
15	Over cut mixed forest	32	Ermans Birch forest
16	Korea pine and broadleaf forest	33	Ermans Birch forest
17	Broadleaf nixed forest	34	Ermans Birch forest

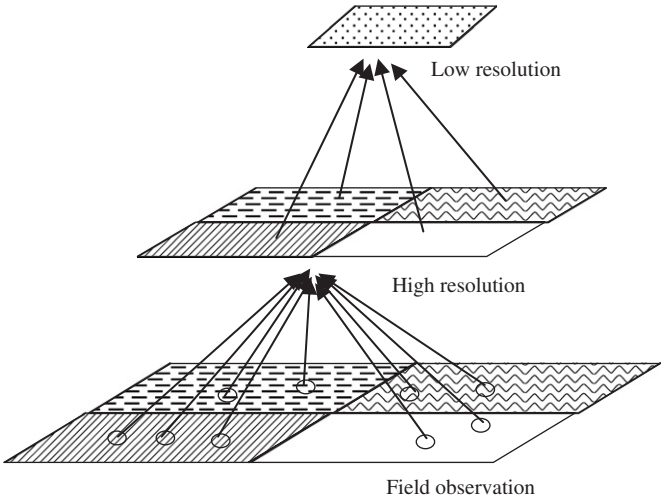

Fig. 7. Validation process.

In Qilian Mountain, the tree species are few and the LAI is small. For the high-resolution satellite image, correlation between SR and LAI was used to map LAI (Fig. 8a). However, in Changbai Mountain, tree species are numerous and given that only a few sample points were obtained for each forest type, the measurements were insufficient to establish a forest type- dependent SR-LAI relationship. The reduced simple ratio (RSR) (Brown et al., 2000) was therefore used in this case (Fig. 8b). The major advantages of RSR over SR are that (i) the information from the background is suppressed, and (ii) the difference between cover types is greatly reduced and can be neglected in many cases; hence LAI can be retrieved from RSR without considering differences among forest types (Brown et al, 2000; Chen et al., 2002).

The LAI of a low-resolution pixel was calculated from the following equation:

$$\mathrm{LAI_L} = \frac{1}{N}\left(\sum_{i=1}^{N} \mathrm{LAI_H}(i)\right), \tag{21}$$

where $\mathrm{LAL_L}$ is LAI of a low-resolution pixel, $\mathrm{LAI_H}(i)$ is the ith high resolution pixel that is part of the low-resolution pixel, and N is the number of high-resolution pixels within a low-resolution pixel. The validation result is illustrated in Fig. 9.

4. Discussion

In the algorithm developed in this study, saturation and background NDVI values for each cover type are predetermined parameters that have considerable effects on the retrieved LAI results. To investigate the influence of these two factors on retrieved LAI, a sensitivity test was conducted. A pixel was randomly selected from the image, and the LAI of the selected pixel was calculated using different combinations of the saturation and background NDVI values. Fig. 10 shows results of the sensitivity test,

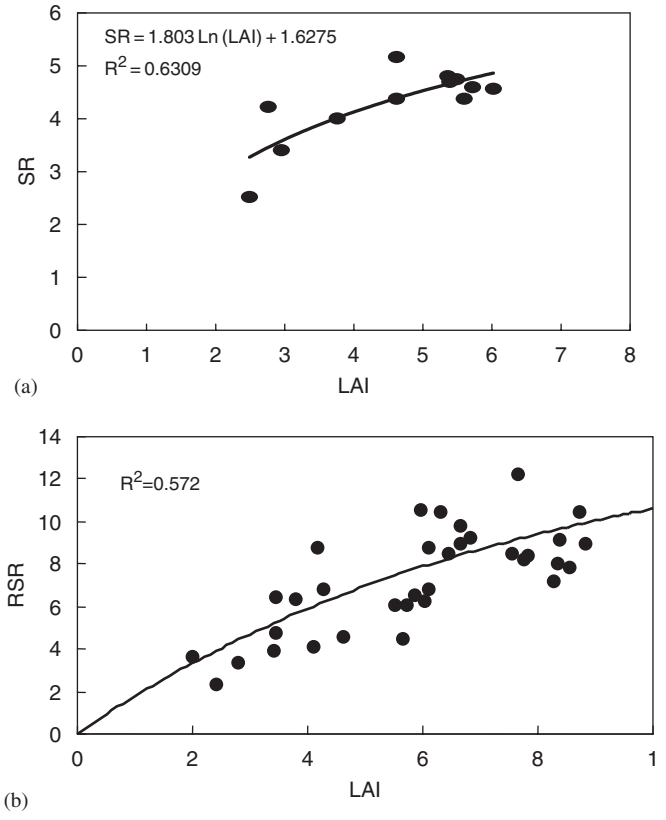

Fig. 8. Relationship between simple ration (SR) and LAI at Qilian Mountain (a); and relationship between reduced simple ration (RSR) and LAI at Changbai Mountain (b).

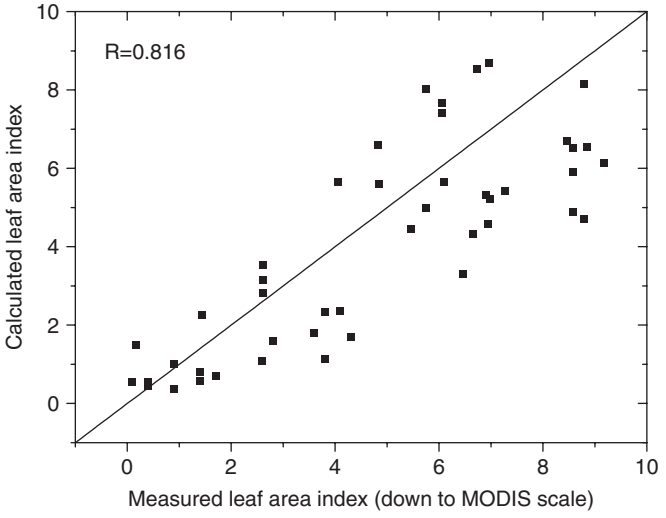

Fig. 9. Validation of 1 km LAI derived using MODIS data against high-resolution LAI maps for two ground sites based on ground measurements.

where the background NDVI varies along the X-axis and the saturation NDVI varies along the Y-axis. The inversion of LAI was not sensitive to the background NDVI, as evidenced by the nearly flat contour lines along the X-axis. For example, when the background NDVI varies from 0 to 0.2, the LAI changes by less than 0.5. This small sensitivity of retrieved LAI to the background NDVI can be

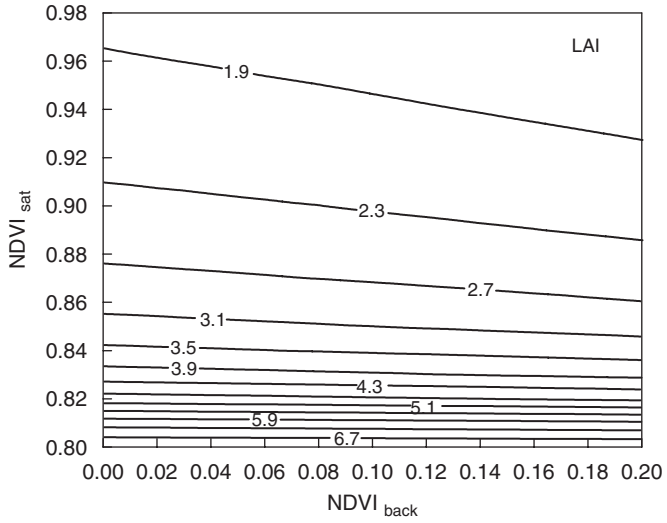

Fig. 10. Influence of saturation and background NDVI on the algorithm.

explained by Eq. (9) and Eq. (20). It is well known that NDVI can partly eliminate the influence of background. In Eq. (20), the background NDVI occurs both in the numerator and the denominator, thus further weakening its effect on the LAI inversion. Therefore, our algorithm reduces the influence of background optical properties.

LAI variation along the *Y*-axis is larger than along the *X*-axis (Fig. 10), indicating that the influence of $NDVI_{sat}$ on LAI is greater than $NDVI_{back}$. The higher the LAI, the denser are the contour lines, and the greater the gradient along the *Y*-axis. The contour lines show that the $NDVI_{sat}$ effect is larger at higher LAI values. At low LAI values, contour lines are very sparse and their gradients small, suggesting that the effect of $NDVI_{sat}$ is small at low LAI values.

The above results imply that the largest error in LAI retrieval occurs for pixels with the NDVI values close to the saturation NDVI. This is an inherent limitation of optical remote sensing, which our algorithm is not able to avoid. In general, the algorithm, through the use of multiple angle information, can overcome problems in mono-angle LAI algorithm caused by the forest background. The major advantage of the new algorithm is that the retrieval error is insensitive to background variability because the latter is automatically taken into account. Higher LAI retrieval accuracy in its application to new areas can be achieved by adjusting the saturation and background NDVI values according to observed data if in situ observations are available.

5. Conclusions

Regional and global retrieval of LAI plays a very important role in numerous remote sensing applications to terrestrial ecosystems. However, obtaining accurate LAI estimates is not an easy task. Some commonly used methods, such as those based on vegetation indices or physical models, often have problems when used in large area applications. Since ground observations for large areas are difficult to acquire, empirical relationships between ground data and coarse resolution remote sensing data are inherently unreliable. The shortcomings of physical model-based methods are also obvious. First, there are no perfect remote sensing forward models that can be directly used for LAI inversion over large areas. Secondly, selection of the parameters for the inversion models is complicated, and some parameters are very difficult to determine. Furthermore, to improve the inversion accuracy, many factors need to be considered, and large lookup tables are needed to support the inversion. For common remote sensing users and regular applications, complex models would not be generally the first choice.

To circumvent some of the above problems, a new LAI inversion method was developed in this paper. Compared with existing approaches, it not only draws on the advantage of vegetation index methods and is simple and easy to use, but also takes advantage of remotely sensed directional characteristics of the plant canopy. The algorithm was validated using data collected in the field. An accuracy of 82% was reached.

The algorithm also provides a new framework for LAI inversion that differs from existing methods. Under this framework, many modules can be further studied and improved, for example, the BRDF algorithm, the gap fraction algorithm, and others. Based on the product evaluation conducted in this study, the current algorithm does not appear to provide significantly better LAI products than existing methods because it depends on the accuracy of the current input products (e.g., the BRDF product for the kernel parameters). However, it is anticipated that as the remote sensing products are improved and the algorithm is further refined, this approach will lead to a more complete and effective utilization of the information content of multiple angle optical remote sensing for terrestrial applications.

Acknowledgments

This research is supported by National Natural Science Foundation of China (Project 40301034 and 40671131), CIDA project, the Special Funds for Major State Basic Research Project (Grant no. G20000779) and the Special Funds of CMA for Climate change. Part of this work was completed while the author was a visiting scholar at the University of Toronto, Canada. We thank Dr. Guowang Qiu for his review and correction on the manuscript.

References

Baret, F., Clevers, J.G.P.W., Steven, M.D., 1995. The robustness of canopy gap fraction estimates from red and near-infrared reflectances: a comparison of approaches. Remote Sensing of Environment 54, 141–151.

Broadhead, J.S., Muxworthy, A.R., Ong, C.K., Black, C.R., 2003. Comparison of methods for determining leaf area in tree rows. Agricultural and Forest Meteorology 115, 151–161.

Brown, I., Chen, J.M., Leblanc, S.G., Cihlar, J., 2000. A shortwave infrared modification to the simple ratio for LAI retrieval in boreal forests: An image and model analysis. Remote Sensing of Environment 71 (1), 16–25.

Chen, J.M., 1999. Spatial scaling of a remotely sensed surface parameter by contexture. Remote Sensing of Environment 69, 30–42.

Chen, J.M., Black, T.A., 1991. Measuring Leaf Area Index of Plant Canopies with Branch Architecture. Agriculture for Meteorology 57, 1–12.

Chen, J.M., Black, T.A., 1992. Defining leaf area index for nonflat leaves. Plant Cell Environment 15, 421–429.

Chen, J.M., Cihlar, J., 1995a. Quantifying the effect of canopy architecture on optical measurements of leaf area index using two gap size analysis methods. IEEE Transactions on Geoscience and Remote Sensing 33 (3), 777–787.

Chen, J.M., Cihlar, J., 1995b. Plant canopy gap-size analysis theory for improving optical measurements of leaf area index. Applied Optics 34 (27), 6211–6222.

Chen, J.M., Leblanc, S.G., 1997. A Four-Scale bidirectional reflectance model based on canopy architecture. IEEE Transactions on Geoscience and Remote Sensing 35 (5), 1316–1337.

Chen, J.M., Leblanc, S.G., 2001. Multiple-scattering scheme useful for hyperspectral geometrical optical modelling. IEEE Transactions on Geoscience and Remote Sensing 39 (5), 1061–1071.

Chen, J.M., Rich, P.M., Gower, S.T., Norman, J.M., Plummer, S., 1997. Leaf area index of boreal forests: Theory, techniques, and measurements. Journal of Geophysical Research 102 (24), 29429–29444.

Chen, J.M., Pavlic, G., Brown, L., Cihlar, J., Leblanc, S.G., White, H.P., Hall, R.J., Peddle, D.R., King, D.J., Trofymow, J.A., Swift, E., Van der Sanden, J., Pellikka, P.K.E., 2002. Derivation and validation of Canada-wide coarse-resolution leaf area index maps using high-resolution satellite imagery and ground measurements. Remote Sensing of Environment 80, 165–184.

Dawson, T.P., Curran, P.J., Plummer, S.E., 1998. LIBERTY—Modelling the effects of leaf biochemistry on reflectance spectra. Remote Sensing of Environment 65, 50–60.

Gao, F., Li, X., Strahler, A.H., Schaaf, C., 2001. Evaluation of the LiTransit Kernel for BRDF Modeling. Remote Sensing Reviews 19, 205–224.

Goel, N.S., 1988. Models of vegetation canopy reflectance and their use in estimation of biophysical parameters from reflectance data. Remote Sensing Reviews 4, 1–213.

Gutman, G., Ignatov, A., 1998. The derivation of the green vegetation fraction from NOAA/AVHRR data for use in numerical weather prediction models. International Journal of Remote Sensing 19, 1533–1543.

Lang, A.R.G., Xiang, Y., 1986. Estimation of leaf area index from transmission of direct sunlight in discontinuous canopies. Agriculture and Forest Meteorology 37, 229–243.

Leblanc, S.G., Chen, J.M., Cihlar, J., 1997. NDVI Directionality in Boreal Forests: a model interpretation of measurements. Canadian Journal of Remote Sensing 23 (4), 369–380.

Leblanc, S.G., Chen, J.M., 2000. A windows graphic user interface (GUI) for the five-scale model for fast BRDF Simulations. Remote Sensing Reviews 19, 293–305.

Leblanc, S.G., Bicheron, P., Chen, J.M., Leroy, M., Cihlar, J., 1999. Investigation of directional reflectance in boreal forests using an improved 4-Scale model and airborne POLDER Data. IEEE Transactions on Geoscience and Remote Sensing 37 (3), 1396–1414.

Leblanc, S.G., Chen, J.M., Kwong M., 2002. Tracing Radiation and Architecture of Canopies. TRAC MANUAL Version 2.1 27.

Li-COR, Inc., 1992. LAI-2000 plant canopy analyzer instruction manual. Li-Cor, NE, USA, pp. 4–12.

Li, X., Strahler, A.H., 1992. Geometric-optical bidirectional reflectance modeling of the discrete crown vegetation canopy: Effect of crown shape and mutual shadowing. IEEE Transactions on Geoscience and Remote Sensing 30 (2), 276–292.

Lucht, W., Schaaf, C.B., Member, IEEE, and Strahler, A.H., Member, IEEE., 2000. An Algorithm for the retrieval of Albedo from space using semiempirical BRDF Models. IEEE Transactions on Geoscience and Remote Sensing 38(2), 977.

Miller, J.B., 1967. A formula for average canopy density. Australian Journal of Botony 12, 141–144.

Ross, J.K., 1981. The Radiation Regime and Architecture of Plant Stands, Dr. W. Junk, Norwell, MA, 392pp.

Roujean, J.-L., Leroy, M., Deschamps, P.Y., 1992. A bidirectional reflectance model of the Earth's surface for the correction of remote sensing data. Journal of Geophysical Research 97, 20455–20468.

Strahler, A., Muchoney, D., Borak, J., Gao, F., Friedl, M., Gopal, S., Hodges, J., Lambin, E., McIver, D., Moody, A., Schaaf, C., Woodcock, C., 1999. MODIS Land Cover Product, Algorithm Theoretical Basis Document (ATBD), Version 5.0, Center for Remote Sensing, Department of Geography, Boston University, Boston, MA. Available from WWW at http://modis.gsfc.nasa.gov/data/atbd/atbd_mod12.pdf

Walthall, C.L., Norman, J.M., Welles, J.M., Campbell, G., Blad, B.L., 1985. Simple equation to approximate the bidirectional reflectance from vegetation canopies and bare soil surfaces. Applied Optics 24, 383–387.

Wanner, W., Li, X., Strahler, A.H., 1995. On the derivation of kernels for kernel-driven models of bidirectional reflectance. Journal of Geophysical Research 100, 21077–21090.

Weiss, M., Baret, F., 1999. Evaluation of canopy biophysical variable retrieval performances from the accumulation of large swath satellite data. Remote Sensing of Environment 70, 293–306.

Welles, J.M., Norman, J.M., 1991. Instrument for indirect measurement of canopy architecture. Agronomy Journal 83, 818–825.

Zeng, X., Dickinson, R.E., Walker, A., Shaikh, M., DeFries, R.S., Qi, J., 2000. Derivation and evaluation of global 1-km fractional vegetation cover data for land modeling. Journal of Applied Meteorlogy 39, 826–839.